Published in final edited form as:

J Am Chem Soc. 2008 December 10; 130(49): 16592–16600. doi:10.1021/ja803556k.

Observing Metal-Catalyzed Chemical Reactions in Situ Using Surface-Enhanced Raman Spectroscopy on Pd–Au Nanoshells

Kimberly N. Heck[†], **Benjamin G. Janesko**[‡], **Gustavo E. Scuseria**[‡], **Naomi J. Halas**[‡,§,‖], and **Michael S. Wong**[†,‡]

Department of Chemical and Biomolecular Engineering, Department of Chemistry, Department of Electrical and Computer Engineering, and Laboratory for Nanophotonics, Rice University, 6100 Main Street, Houston, Texas 77005-1892

Naomi J. Halas: halas@rice.edu; Michael S. Wong: mswong@rice.edu

Abstract

Insight into the nature of transient reaction intermediates and mechanistic pathways involved in heterogeneously catalyzed chemical reactions is obtainable from a number of surface spectroscopic techniques. Carrying out these investigations under actual reaction conditions is preferred but remains challenging, especially for catalytic reactions that occur in water. Here, we report the direct spectroscopic study of the catalytic hydrodechlorination of 1,1-dichloroethene in H_2O using surface-enhanced Raman spectroscopy (SERS). With Pd islands grown on Au nanoshell films, this reaction can be followed in situ using SERS, exploiting the high enhancements and large active area of Au nanoshell SERS substrates, the transparency of Raman spectroscopy to aqueous solvents, and the catalytic activity enhancement of Pd by the underlying Au metal. The formation and subsequent transformation of several adsorbate species was observed. These results provide the first direct evidence of the room-temperature catalytic hydrodechlorination of a chlorinated solvent, a potentially important pathway for groundwater cleanup, as a sequence of dechlorination and hydrogenation steps. More broadly, the results highlight the exciting prospects of studying catalytic processes in water in situ, like those involved in biomass conversion and proton-exchange membrane fuel cells.

Correspondence to: Naomi J. Halas, halas@rice.edu; Michael S. Wong, mswong@rice.edu.

[†]Department of Chemical and Biomolecular Engineering.

[‡]Department of Chemistry.

[§]Department of Electrical and Computer Engineering.

[‖]Laboratory for Nanophotonics.

Supporting Information Available: Description of DFT calculations on chemisorbed 1,1-DCE, with Table S1 (calculated (B3LYP) and experimental vibrational frequencies of 1,1-DCE, and assignments) and Table S2 (selected vibrational frequencies calculated for adsorbates on Pd cluster models); Figure S1 (SEM images of Au NSs and Pd/Au NSs, and EDS of Pd/Au NSs); Figure S2 (schematic of flow chamber); Figure S3 (waterfall plot of chemisorption of 254.4 μM 1,1-DCE followed by the addition of 81 mM H_2 in H_2O); Figure S4 (waterfall plot of chemisorption of 254.4 μM 1,1-DCE followed by the addition of N_2 saturated water); Figure S5 (waterfall plot of chemisorption of 254.4 μM 1,1-DCE over Au NSs); and references. This material is available free of charge via the Internet at http://pubs.acs.org.

JA803556K

1. Introduction

Characterization of the binding and/or reaction of adsorbates at the surfaces of platinum group metals is of great importance for the understanding and improvement of catalytic reactions. Electron energy loss spectroscopy (EELS), for example, is highly satisfactory in detecting molecules bound to model surfaces, but suffers from the need for expensive equipment and ultrahigh vacuum environments. Hence, it cannot be used to replicate actual behavior of catalytic reactions that occur at or above atmospheric pressure or in the presence of a liquid. Fourier transform infrared spectroscopy (FTIR), often coupled with the use of attenuated total reflectance (ATR) techniques and Raman spectroscopy, has also been used to characterize adsorption processes, but the technique is not surface selective, and signal-to-noise ratios often suffer from solvent effects. Moreover, with the growing trend toward greener aqueous-based reactions, the technique is especially limited by the strong IR absorption of the O–H stretching modes of water.[1] Additionally, current techniques often require integration times much longer than actual reaction times. There is a critical unmet need for sensitive, surface-selective, and easy-to-implement methods to provide detailed molecular-level information on heterogeneous catalytic reactions while they occur under realistic reaction conditions.[2–6]

Discovered in the late 1970s, surface-enhanced Raman spectroscopy (SERS) is a strong candidate to fulfill this need.[2,7–10] Raman spectroscopy detects molecules with chemical bonds that exhibit changes in polarizability, and SERS provides orders-of-magnitude improvement in detection limit through the use of nanostructured metal substrates. The primary mechanism responsible for the surface enhancement is the ability of the metal to support directly excitable surface plasmons at the excitation laser wavelength and across the Stokes frequency range. This plasmon response provides an intense electromagnetic field at the metal surface at both the excitation and the Stokes wavelengths.[11] Traditional SERS substrates, such as roughened metal electrodes and aggregated metal nanoparticles, typically offer moderate enhancements of up to 10^6.

With recent developments in understanding structure effects on plasmonic behavior in metal nanostructure synthesis, SERS substrates with higher and more highly reproducible enhancements can be designed.[12] Engineered substrates based on nanometer-sized metallic shapes, like rods, rings,[13] gaps,[14] bowties,[15] and shells,[16] offer SERS enhancements of up to 10^9. In particular, Au nanoshell (NS) SERS substrates have been successfully used to determine conformation of surface-bound biomolecules[17,18] and to transduce the spectral signature of surface-bound thiols in a high-resolution all-optical pH nanosensing device.[19] The large active area for SERS on nanoshell surfaces, along with the large and highly reproducible enhancements designed into these structures, provide a SERS-active substrate that is quite promising for monitoring catalytic processes.

Weaver and others have carried out extensive SERS investigations of catalytic metals, focusing primarily on aqueous-phase electrocatalytic interfaces in which the substrates were roughened noble metal electrodes or nanoparticles coated with 1–2 nm of catalytic metal.[20–24] Some of the reports detailed the adsorption characteristics of catalytically relevant molecules, such as ethylene, methanol, and carbon monoxide, as a function of

electrode potential; evidence of possibly catalyzed molecular transformations was seen (for reviews, see refs [20], [21], [24]). More recently, structured substrates consisting solely of the catalytic material have been introduced.[25,26] These materials approaches offer enhancements of 10^4–10^6, although spectral and temporal resolution remains limited. Engineered substrates, thus far, have not been developed for studying or monitoring catalytic reactions.

In this study, catalytically responsive and SERS-active functionalities were combined in a single substrate by depositing Pd (the catalytic surface) onto Au nanoshells (the SERS substrate). This structure is based on our recent reports of the unexpectedly high activity of Au nanoparticles coated with a submonolayer of Pd metal for the room-temperature, aqueous-phase hydrodechlorination (HDC) of trichloroethene (TCE).[27,28] Gold likely enhances Pd catalysis through geometric and mixed site effects; electronic effects may play a factor also. With important implications for groundwater treatment, these Pd-on-Au nanoparticle (Pd/Au NP) catalysts are highly efficient for perchloroethene (PCE) and other water-borne contaminants and are more resistant to poisoning as compared to Pd-only catalysts.[29] It has been proposed previously that TCE degrades through sequential dechlorination and hydrogenation steps, but evidence has been lacking. By combining the nanoshell SERS sensing geometry with submonolayer Pd deposition, this same enhanced catalytic activity can now be monitored in situ using SERS.

2. Experimental Section

2.1. Preparation of Au NS and Pd/Au NS

The multistep preparation is detailed as follows (Figure 1a). Au nanoshells (NSs) were prepared as described previously.[16] Briefly, 1 mL of 120 nm diameter silica colloid (Precision colloid P120) was added to 26 mM aminopropyltrimethoxysilane in ethanol and aged overnight. The solution (500 μL) was then added to 40 mL of a sol of 1–2 nm Au NPs, previously prepared via the Duff method[30] and aged for at least 2 weeks. The sample was aged overnight to allow the electrostatic self-assembly of the negatively charged Au NPs to the positively charged amine groups on the modified silica colloid. The sample was then centrifuged and redispersed in deionized water three times to ensure the removal of excess Au NPs, leaving a final volume of ~1 mL. The sample (15 μL) was added to 3 mL of an aqueous solution of 370 μM $HAuCl_4$ and 18 mM K_2CO_3 and was stirred. The gold salt was then reduced onto the silica cores by adding 30 μL of 30 wt % formaldehyde and shaking vigorously for 5 min. The sample was then centrifuged and redispersed in deionized water to ensure the removal of excess gold salt. The final volume of the solution was 3 mL.

The UV–visible spectrum of the Au NSs was fit using Mie scattering theory to determine the size and concentration of particles. Quantitative agreement between experimental and theoretical NS spectra was obtained for 60 nm radius SiO_2 core and 22 nm Au shell thickness (Figure 2a,b), with the overall radius of 82 nm confirmed by analyzing 200 particles with SEM (Figure S1). The concentration of NSs was determined to be 1.18×10^8 particles/mL.

Au NSs coated with a submonolayer of Pd metal (Pd/Au NSs) were synthesized analogously to the previously reported synthesis of Pd/Au NPs.[28] H_2PdCl_4 (7.2 μL of 2.4 mM solution)

was added to 18 mL of the as-synthesized Au NSs and stirred. The Pd salt was reduced by bubbling the solution with UHP H_2 gas for 5 min.

Scanning electron microscope (SEM) images and electron dispersive X-ray (EDX) spectra of the Pd/Au NSs were obtained using a FEI Quanta 400. For particle size analysis, 30 μL of either Au NSs or Pd/Au NSs was drop-dried onto an SEM stub. For EDX analysis, Pd/Au NSs were repeatedly drop-dried onto a stub until a visibly thick layer was formed. The spectrum was obtained using an EDX detector attached to the SEM.

To characterize any changes in plasmonic behavior upon the addition of Pd, UV–vis absorbance spectra of the NSs were collected on a Shimadzu UV-2401 PC spectrophotometer using a polystyrene cuvette with a 1 cm path length.

2.2. Preparation of Samples for SERS Analysis

To immobilize the NSs, 5 mm × 5 mm × 0.5 mm polished Si wafers were cleaned in 3:7 solution of 30 wt % H_2O_2 and 30 wt % H_2SO_4 for 1 h. The wafers were then rinsed in deionized water and dried, before being added to a solution of 0.1 wt % poly(vinylpyridine) (MW ~40 000) in ethanol. After aging overnight, the wafers were rinsed in ethanol and dried. 50 μL of a concentrated solution of the NSs (volume reduced from 18 mL to 128 μL by centrifugation and removal of supernatant) was then pipetted onto a wafer and allowed to assemble overnight, schematically shown in Figure 1b. After being rinsed with deionized water to remove unattached NSs, the wafer was adhered to the center of an 18 mm round microscope coverslip using slide adhesive. Samples used in the reaction and chemisorption experiments were then plasma-cleaned under vacuum (Harrick Plasma Cleaner/Sterilizer, PDC-32G) to remove surface impurities for 2 min just prior to Raman analysis.

2.3. Characterization of SERS Effectiveness

To determine the SERS effectiveness of Pd/Au NSs relative to the Au NSs, 10 μL of 440 μM *para*-mercaptoaniline (pMA) in ethanol was added to samples prepared as in the previous section. pMA is a highly Raman active species and has been used in a number of experiments to determine SERS efficiency.[31] The samples were aged overnight to ensure the formation of a complete monolayer on the nanoshell surfaces in parafilm-sealed Petri dishes and then rinsed with ethanol prior to analysis.

SERS spectra were obtained using a Renishaw inVia micro-Raman spectrometer with a 785 nm excitation laser and a 40× working distance objective. Spectra were obtained using 0.05 mW power and 10 s integration times. For each sample, eight spectra were acquired at different spots and averaged. The standard deviation between spectra for each sample was less than 5%.

2.4. SERS Monitoring of Adsorption and Reaction of 1,1-DCE

To perform the adsorption (or chemisorption) and reaction experiments, the plasma-cleaned sample was mounted in a sealed analysis chamber with inlet and outlet ports (Warner Instruments RC-43, 213 μL volume without Pd/Au NS sample) and mounted inside the Raman spectrometer (Figure S2). Prior to the acquisition of spectra from the substrate, the

reduction of Pd was ensured by flowing 10 mL of H_2 saturated deionized H_2O and allowing it to sit for 10 min.

We chose to study 1,1-DCE (1,1-dichloroethene), a less chlorinated form of TCE that lends itself to simpler spectral interpretations and that is hypothesized to be a reaction intermediate for TCE HDC. Solvents used to perform the chemisorption and reaction experiments were prepared by adding 180 mL of deionized water each to Boston Round screw top bottles (Alltech, 250 mL). The threads were wrapped with Teflon tape and sealed with a Teflon-rubber septum. Two bottles (one used for catalyst rereduction and the other for rinsing) were bubbled with UHP H_2 and N_2, respectively, for 1 h. Additional bottles were bubbled for 1 h with N_2 or with H_2:N_2 gas mixtures (volume ratios of 20:80 and 100:0) for use in the chemisorption and/or reaction experiments. The H_2 concentrations present in the aqueous phase were estimated to be 16.3 and 81.9 mM, respectively, using a Henry's law constant of 1228 atm/M. After the bubbling step, 1 or 5 μL of 1,1-DCE was added, such that the H_2:1,1-DCE molar ratio was the same; the amount of 1,1-DCE dissolved in the liquid phase was estimated to be 50.9 or 254.5 μM, respectively, using a Henry's law constant of 26.1 atm/M and a density of 1.21 g/L. The liquid-phase H_2 amount was set approximately 6% in excess to what is needed for complete conversion of 1,1-DCE to ethane ($CH_2{=}CCl_2 + 3H_2 \rightarrow CH_3CH_3 + 2HCl$). The bottles were placed on a rocking platform to allow dissolution and equilibration of 1,1-DCE between the gas and liquid phases.

Spectra ranging from 100 to 1700 cm^{-1} Raman shifts were obtained using 0.76 mW of laser power and 10 s integration times, a total acquisition time of 1 min per spectrum. Ten spectra were obtained at a single spot prior to the changing of solvents to establish a baseline and ensure the cleanliness of the substrate.

For the chemisorption experiments, the analysis chamber was first flushed with N_2-saturated H_2O to remove excess H_2 from the cell, and to remove possible chemisorbed H_2. The chamber was then flushed with 3 mL of the N_2-saturated 1,1-DCE solution (50.9 or 254.5 μM), and spectra were collected over time. Similar experiments were performed using Au NSs (without Pd metal).

Experiments involving a chemisorption-reaction sequence were performed similarly. After the sample was flushed with N_2-saturated H_2O, 3 mL of the 254.5 μM sample was added. Spectra were obtained repeatedly for 30 min, after which 1 mL of either 0:100, 25:75, or 30:70 H_2:N_2 was quickly flushed through the cell, and spectra were taken continuously until no other changes occurred.

For the reaction experiments, 3 mL of low-concentration (1,1-DCE, 50.9 μM; H_2, 16.3 mM) or high-concentration (1,1-DCE, 254.5 μM; H_2, 81.9 mM) solutions was added, and spectra were collected over time until no noticeable changes in the spectra were observed.

Baseline corrections in the spectra were performed by normalizing to the silicon 520 cm^{-1} mode, to account for any minor drifts in focus over the experimental time frame. The baseline was corrected by subtracting an average of the initial 10 spectra taken to determine surface cleanliness.

2.5. Analysis of Bulk Reaction Products

To analyze the products using the SERS analysis chamber, the same protocol was used as in the SERS reaction experiments, except that aliquots of fluid were removed (~200 μL) at 0, 12, 30, 41, or 100 min with a 1 mL needled syringe and injected into a 2 mL septum-capped vial. After the gas and liquid phases of the sample were allowed to equilibrate for 30 min, 250 μL of headspace gas was withdrawn with a gastight syringe and injected into an Agilent Technologies 6890 GC equipped with a flame ionization detector (FID) and a packed column (6 in. × 1/8 in. outer diameter) containing 60/80 Carbopack B/1% SP-1000 (Supelco). Calibration curves were prepared for chlorinated ethenes, chlorinated ethanes, ethane, and butane. The zero time point samples were verified to match the initial 1,1-DCE concentrations of 50.9 and 254.5 μM for the low-and high-concentration experiments, respectively.

Upon analysis of the products, it became apparent that, at later time points, the carbon balance did not always close, possibly due to evaporation from the gastight syringe before injection into the GC. To correct for this, we assumed evaporation of all components was equal and rescaled the measured concentrations with the same correction factor, such that the total carbon balance was met for all time points.

The superficial first-order rate constant was determined by linear fitting of $\ln(C/C_0)$ versus time profiles, where C is 1,1-DCE concentration and C_0 is the initial 1,1-DCE concentration. Selectivities were calculated by dividing the concentration of each product by the amount of 1,1-DCE reacted.

3. Results and Discussion

3.1. Characterization of SERS Efficiency

The average Pd/Au NS diameter was found to be 164 nm, according to SEM analysis (Figure 1c), indicating no detectible size increase after the addition of Pd metal. Electron dispersive X-ray (EDX) spectroscopy confirmed the presence of Pd (Figure S1). We estimated that the Au NS surfaces had a ~10% coverage of Pd atoms (meaning ~10% of complete Pd monolayer coverage). The final composition of the Pd-decorated Au NSs was estimated at 6.7 wt % SiO_2, 90.6 wt % Au, and 2.7 wt % Pd.

The plasmon resonance spectrum of the Au NSs decreased in intensity and red-shifted slightly with the addition of the Pd metal, similar to what had been observed with Pd-coated Au NPs.[27,32] The relatively large imaginary part of the Pd dielectric constant in the visible light regime damps the plasmon resonance, as seen in the Mie theoretical modeling of Au nanoshells with 100% Pd coverage (Figure 2b).

The intensity of the SERS spectrum obtained from pMA-functionalized Au and Pd/Au NSs decreased with the presence of Pd on the NS surface due to damping of the Au NS plasmon resonance (Figure 2c). An interesting feature of this SERS spectrum is the shift in the intense, low-frequency peak near 390 cm^{-1} (Figure 2c, inset). This vibrational mode was assigned to coupling between the metal–sulfur bond stretch and a pMA ring deformation.[33]

This peak shifted to 406 cm^{-1} with the addition of Pd, indicating an increase in the surface–pMA bond strength and the possible binding of pMA to Pd surface atoms.

3.2. Adsorption of 1,1-DCE

Figure 2d shows the SERS spectra for 1,1-DCE over Au and Pd/Au NSs. In contrast to the pMA case, it is readily apparent that Pd increased the 1,1-DCE band intensities despite the damping effect of Pd on Au NS extinction.

Figure 3a–c shows the results of contacting the Pd/Au NSs with an aqueous solution of 1,1-DCE at 50.9 μM. After an induction period, there appeared to be two different time-dependent adsorption states: the initial state (0–20 min; Figure 3b), with Raman spectra featuring bands at 214, 954, ~1060, ~1160, ~1250, 1430, and 1550 cm^{-1}, and the final state (37–52 min; Figure 3c), with bands found at ~225, ~390, ~1165, ~1455, and ~1500 cm^{-1}. The peaks can be assigned to wavenumber regions that represent particular Raman-active vibrational modes of surface-bound 1,1-DCE, based on reported assignments for chemisorbed ethylene,[34] TCE,[35] free 1,1-DCE,[36] and corroborated with ab initio density functional theory calculations (Supporting Information). Peaks in the 1500–1600, 1220–1290, and 1000–1100 cm^{-1} range were assigned to CC stretching, CH_2 scissoring, and CH_2 wagging modes of π-bound 1,1-DCE, respectively. The sharp peaks at 954, ~1160, and 1430 cm^{-1} were further assigned to the CC stretching, CH_2 wagging, and CH_2 scissoring modes of di-σ-bound 1,1-DCE. The other closely located peaks suggest different metal adsorption sites, sites of different binding strengths, or binding states intermediate to those of the π- and di-σ-bound 1,1-DCE species. The low-frequency features below 400 cm^{-1} may be due to C–M (M = metal) or C–Cl bonds. These results provide direct evidence of 1,1-DCE undergoing chemisorption from water.

1,1-DCE adsorption is dynamic, as the initial state changes substantially into a new stable state (Figure 3a). Signals for π-bound 1,1-DCE were lost, with residual di-σ-bound 1,1-DCE showing the weak peaks at ~1165 and ~1455 cm^{-1}. A sharp and intense peak at ~1500 cm^{-1} may be due to the CC stretch of vinylidene (=C=CH_2) species; this value is slightly blue-shifted from the theoretical value of 1490 cm^{-1} for vinylidene on Pd(111)[37] and red-shifted from that for vinylidene on Si surfaces,[38] and in the range predicted by our ab initio calculations. The bands at 230 and ~390 cm^{-1} can be attributed to Cl–M and C–M bond stretchings, respectively, consistent with the removal of chlorine from 1,1-DCE to form vinylidene. This process is summarized in Scheme 1.

Figure 3d–f shows the results of contacting the Pd/Au NSs with an aqueous solution of 1,1-DCE at a higher concentration of 254.5 μM. Unlike the 50.9 μM case, Raman peaks appeared almost immediately after injection of the DCE solution. The peaks at ~220 and ~400 cm^{-1} (Cl–M and C–M bond stretchings) indicated DCE dechlorination. Bands centered at ~1500 and ~1200 cm^{-1} were quite broad, spanning at least 100 cm^{-1}, suggesting vinylidene and other adsorbed species. The band positions did not change much with time, but their intensities increased continuously until ~20 min, after which the spectra stabilized. It is likely that the broad band at ~1500 cm^{-1} represents unsaturated oligomeric species on the metal surface, as they have previously been assigned to conjugated olefins.[39,40] This is not unexpected, as previous kinetic studies with TCE using Pd-based[41,42] and Pd/Au-

based[28] catalysts have reported trace amounts of carbon-coupling products at low H_2/TCE concentration ratios. These olefinic species were observed due to the higher DCE surface concentration, leading to increased interactions between chemisorbed DCE species (i.e., surface crowding effect). These species could be removed from the NS surface by contacting with H_2-containing water (Figure S3) but not with N_2-containing water (Figure S4).

Control experiments using Au-only NSs and 50.9 μM (Figure 2d) and 254.5 μM DCE (Figure S5) solutions showed no Raman peaks at all. These results indicated that solvated 1,1-DCE could not be detected at these concentrations and was observable only in the presence of Pd metal, suggesting Pd ensembles or Pd–Au mixed sites as active sites for chemisorption. While the surface structure of Pd on the Au NSs is not known precisely, the metal most likely is present as two-dimensional atomic ensembles or islands.[29,43]

3.3. Reaction of 1,1-DCE

For the experiment using the 50.9 μM DCE and 16.3 mM H_2 solution, the resulting spectra differ dramatically from the non-H_2 case, with Raman peaks (additional to those associated with π-bound and di-σ-bound DCE) appearing and changing rapidly with time (Figure 4a–e). We hypothesized that H_2 dissociatively adsorbed to form atomic H species, which would accelerate the dechlorination of adsorbed DCE. The vinylidene species may have been present (~1480 cm^{-1}) with dechlorination occurring as early as 5 min after H_2 introduction, inferred from the appearance of broad bands below 400 cm^{-1} (Cl–M and C–M bonds). In contrast, dechlorination was not observed until 20 min when there was no H_2 (Figure 3b). Vinyl surface species (–HC=CH_2) may have been present also, with small features at ~1230, ~1360, and ~1580 cm^{-1} that represent CC–CH bending, CH_2 scissoring, and CC stretching, respectively,[44] which would have formed from vinylidene hydrogenation (Figure 4b). Ethylidyne (≡C–CH_3, with a CC stretch at 1118 cm^{-1} and CH_3 umbrella mode at 1326 cm^{-1}[45]) is a different vinylidene hydrogenation product but was not detected.[44] Further hydrogenation led to π- and di-σ-bound ethene, which could have contributed to the peaks close to those of π- and di-σ-bound DCE. Intriguingly, the distinct peak at 1193 cm^{-1} may be assigned to an ethyl surface species (–CH_2CH_3, CH_2 wagging mode), resulting from hydrogenation of adsorbed ethene.[46] Peaks were detected in the 600–900 cm^{-1} range (C–Cl stretches from the population of chlorinated surface species), but were not detected in the absence of H_2 (Figure 3b), suggestive of partially dechlorinated 1,1-DCE surface species.

While more specific peak assignments could not be obtained, general trends in the SERS spectra were observed with increasing time (Figure 4a). The ~250 cm^{-1} peak (M–Cl) increased and then slightly decreased after 30 min, suggesting that surface Cl eventually hydrogenated to form HCl, which then desorbed into the water phase. The peaks in the 600–900 cm^{-1} range (C–Cl) disappeared by 41 min, indicating complete dechlorination of surface species. The 1100–1600 cm^{-1} range became more intense, with broad peaks centered ~1200 and ~1500 cm^{-1} similar to those observed in the absence of H_2 at a higher 1,1-DCE concentration (Figure 3f). The peak at ~1530 cm^{-1} could be the CC stretch of a well-defined longer-chain olefinic surface species. Changes in the SERS spectra seemingly terminated at 41 min, likely due to blockage of catalytic sites by olefinic species and adsorbed Cl. This observation did not signify that the catalytic reaction terminated at 41 min,

as reaction products still formed at 100 min (as shown in the next section). Rather, it indicated that the signals for the oligomeric species dominated those of surface intermediates directly involved in catalytic reaction pathway.

Similar trends were observed in the SERS spectra when DCE and H_2 concentrations were increased by 5-fold (Figure 4f–j). The resulting higher concentrations of surface species led to increased reaction rates, as shown by the more intense ~240 and 400 cm^{-1} peaks (Cl–M and C–M stretches). New peaks at ~1115 and ~1330 cm^{-1} were found at early reaction times,[45] indicative of ethylidyne species that were absent at lower reactant concentrations.

3.4. Analysis of 1,1-DCE HDC Bulk Reaction Products

To confirm that the HDC reaction was occurring during SERS analysis, we removed and analyzed the aqueous-phase content of the SERS chamber at 0, 12, 30, 41, and 100 min. For both low- and high-concentration conditions, 1,1-DCE concentrations decreased with 100% selectivity toward ethane production; 1,1-DCE conversion reached 9% by 30 min (Figure 5). Beyond 30 min for the low-concentration experiment, 1,1-DCE reacted more slowly (vide infra) and ethane selectivity dropped to 95% as ethene began to form, attributed to reduced H_2 reactant concentration. The product concentrations did not change much from 41 to 100 min. Combined with the SERS observations in the same time range (Figures 4a), vinylidene and longer-chain olefinic as well as chloride surface species may be blocking enough active sites to slow 1,1-DCE consumption. Deactivation due to surface site blockage likely is responsible for observed slower reaction kinetics beyond 30 min (above 9% conversion of 1,1-DCE).

Beyond 30 min for the high-concentration experiment, 1,1-DCE also reacted more slowly and ethane selectivity dropped to 95% as ethene and C_4 molecules (butanes and butanes, which we did not further differentiate due to experimental limitations) began to form. Vinyl chloride (from incomplete dechlorination of 1,1-DCE) and 1,1-dichloroethane (from hydrogenation of 1,1-DCE) are theoretical byproduct; they were not detected though, consistent with that observed with Pd/Au NPs.[27–29] Carbon-coupling reactions led to the olefinic surface species observed via SERS at low and high reactant concentrations (Figure 4), and to C_4 reaction products only in the latter case (Figure 5c,d). The C_4's appeared in parallel with ethene, indicating that both originated from the same surface species.

We considered the decrease in 1,1-DCE concentration to follow an exponential trend through 30 min. The implication that the HDC reaction was first-order in 1,1-DCE and zero-order in H_2 was reasonable, given the low extent of reaction (<9% conversion). For both low and high reactant concentration conditions, an approximate rate constant of 0.003 min^{-1} was calculated, giving a lower-bound estimate of initial reaction rate constant of 0.872 $L/g_{Pd}/min$ (assuming no NSs were lost during preparation and experimentation). The initial turnover frequencies (=1,1-DCE molecules initially reacted per Pd atom per min) for the low and high reactant concentrations were 0.0047 and 0.023 min^{-1}, respectively.

The turnover numbers (TON = total number of 1,1-DCE molecules reacted per Pd atom) at the low and high reactant concentration cases at 100 min were calculated to be 0.17 (=1.17 nmol of DCE reacted ÷ 6.89 nmol of Pd) and 1.21 (=8.3 nmol of DCE reacted ÷ 6.89 nmol

of Pd), respectively. That TON exceeded 1 proved that the nanoshells are catalytically active for HDC. We note that TON can be calculated to be <1 for catalyzed reactions when rates are slow or at short reaction times. These cases occurred in our study involving low and high reactant concentrations, respectively.

To note, Pd/Au NPs (25% Pd coverage) have a rate constant of 1519 $L/g_{Pd}/min$ for 1,1-DCE HDC,[29] allowing us to estimate that Pd/Au NPs (10% Pd coverage) have a rate constant of ~600 $L/g_{Pd}/min$, much higher than the 0.872 $L/g_{Pd}/min$ for Pd/Au NSs (10% Pd coverage). However, this is an incompatible comparison because the reaction conditions were very different. The Pd/Au NSs were immobilized on a surface during catalysis, and the H_2 reactant amount was 6% in excess of the stoichiometric amount needed for complete reaction of 1,1-DCE. In contrast, Pd/Au NPs were stably dispersed in water during batch reactor kinetic studies,[27,28] and 1,1-DCE and H_2 concentrations were 77% and 2416% respectively higher; the H_2 amount was ~1400% in excess of the stoichiometric amount needed.[29]

Summarizing the spectroscopic and bulk reaction data together, we propose a simple model of the 1,1-DCE HDC reaction on Pd/Au NSs as a series of surface reactions (Scheme 2). 1,1-DCE chemisorbs in two different binding states, eventually dechlorinating to form vinylidene species. Vinylidene then hydrogenates to form ethylidyne (at high precursor concentration) and vinyl intermediates. Surface oligomers form detectibly as spectator species from the carbon coupling of, perhaps, vinylidene groups. Ethylidyne can hydrogenate to form ethane but at a rate much slower than is observed spectroscopically, and so it may be a spectator species here also.[46,47] In contrast, the vinyl group hydrogenates to form surface-bound ethene. Its hydrogenation then occurs to form the ethane product (detectible through gas chromatography but not through SERS) via the classical Polanyi–Horiuti pathway, that is, surface ethene → surface ethyl → surface ethane → desorbed ethane.[48,49] The consumption of 1,1-DCE leads to the quantitative formation of ethane, until surface site blockage by oligomeric or chloride species slows hydrogenation kinetics sufficiently for surface-bound ethene to desorb into the water phase as a product. High 1,1-DCE reactant concentrations lead to high surface species concentrations, with surface site blockage leading to side-product formation of C_4's in addition to ethene.

4. Conclusions

This study shows the successful synthesis and application of Pd-supported Au NSs for the detection of water-phase adsorbates. The Pd metal provided direct binding sites on the Au surface (either as Pd ensembles or as Pd–Au mixed sites), effectively lowering the concentration detection limit for SERS. Significantly, chemical reactions of adsorbate species can be observed as they proceed on the catalyst surface with time, providing a newfound ability to detect and identify reaction intermediates in water under ambient conditions in situ. With further development in improved time and Raman peak resolutions under steady-state flow conditions, NS-enabled SERS may lead to new mechanistic insights into other liquid-phase chemical reactions, like gold-catalyzed glycerol oxidation and platinum-catalyzed electroreduction of oxygen, for which spectroscopic analysis is lacking. Presented here is the first spectroscopic evidence of water-phase hydrodechlorination as a

sequence of dechlorination and hydrogenation steps, leading to the implication that 1,1-DCE, TCE, PCE, and other related contaminants degrade in a similar fashion using Pd-supported Au NP catalysts.

Supplementary Material

Refer to Web version on PubMed Central for supplementary material.

Acknowledgments

This work is supported by the NSF (IGERT, DGE-0504425; CBEN, EEC-0647452). B.G.J. is supported by a training fellowship from the National Library of Medicine to the Keck Center for Interdisciplinary Bioscience Training of the Gulf Coast Consortium (NLM Grant No. 5T15LM07093). G.E.S. acknowledges support from NSF CHE-0807194 and the Welch Foundation (C-0036). M.S.W. acknowledges additional support from the Welch Foundation (C-1676) and SABIC Americas. N.J.H. acknowledges additional support by Air Force Office of Scientific Research Grant (F49620-03-C-0068), the Texas Institute for Bio-Nano Materials and Structures for Aerospace Vehicles funded by NASA Cooperative Agreement (No. NCC-1-02038), the Robert A. Welch Foundation (C-1220), and the Multidisciplinary University Research Initiative (MURI) Grant (W911NF-04-01-0203). We thank Prof. Jason Hafner for helpful discussions and generous use of his plasma cleaner.

References

1. Somorjai, G. Introduction to Surface Chemistry and Catalysis. Wiley Interscience; New York: 1994.
2. Jeanmaire DL, Van Duyne RP. J Electroanal Chem. 1977; 84:1–20.
3. Banares MA. Catal Today. 2005; 100:71–77.
4. Wachs IE. Catal Commun. 2003; 4:567–570.
5. Weckhuysen BM. Chem Commun. 2002; 2:97–110.
6. Haw, JF. In-Situ Spectroscopy in Heterogeneous Catalysis. Wiley; New York: 2002. p. 288
7. Mrozek MF, Weaver MJ. J Phys Chem B. 2001; 105:8931–8937.
8. Tian ZQ, Wu DY. J Phys Chem B. 2002; 37:9363–9483.
9. Beltramo GL, Shubina TE, Koper MTM. ChemPhysChem. 2005; 6:2597–2606. [PubMed: 16331729]
10. Chan HYH, Williams CT, Weaver MJ, Takoudis CG. J Catal. 1998; 174:191–200.
11. Kerker M, Wang DS, Chew H. Appl Opt. 1980; 24:4159–4174. [PubMed: 20309031]
12. Lal S, Grady NK, Kundu J, Levin CS, Lassiter JB, Halas NJ. Chem Soc Rev. 2008; 37:898–911. [PubMed: 18443675]
13. Aizpurua J, Hanarp P, Sutherland DS, Kall M, Bryant GW, de Abajo FJG. Phys Rev Lett. 2003; 90:5.
14. Ward DR, Grady NK, Levin CS, Halas NJ, Wu YP, Nordlander P, Natelson D. Nano Lett. 2007; 7:1396–1400. [PubMed: 17430009]
15. Fromm DP, Sundaramurthy A, Kinkhabwala A, Schuck PJ, Kino GS, Moerner WE. J Chem Phys. 2006; 124
16. Oldenburg SJ, Averitt RD, Westcott SL, Halas NJ. Chem Phys Lett. 1998; 288:243–247.
17. Levin CS, Grady N, Halas N. Anal Chem. 2006; 78:3277–3281. [PubMed: 16689527]
18. Barhoumi A, Zhang D, Tam F, Halas NJ. J Am Chem Soc. 2008; 130:5523–5529. [PubMed: 18373341]
19. Bishnoi S, Gheith M, Johnson B, Rozell D, Johnson D, Halas N. Nano Lett. 2006; 6:1687–1692. [PubMed: 16895357]
20. Weaver MJ. J Raman Spectrosc. 2002; 33:309–317.
21. Weaver MJ. Top Catal. 1999; 8:65–73.
22. Gomez R, Solla-Gullon J, Perez JM, Aldaz A. J Raman Spectrosc. 2005; 36:613–622.
23. Fokas C, Deckert V. Appl Spectrosc. 2002; 56:192–199.

24. Tian ZQ, Ren B. Annu Rev Phys Chem. 2004; 55:197–229. [PubMed: 15117252]
25. Abdelsalam ME, Mahajan S, Bartlett PN, Baumberg JJ, Russell AE. J Am Chem Soc. 2007; 129:7399–7406. [PubMed: 17506559]
26. Xiong YJ, McLellan JM, Chen JY, Yin YD, Li ZY, Xia YN. J Am Chem Soc. 2005; 127:17118–17127. [PubMed: 16316260]
27. Nutt MO, Hughes JB, Wong MS. Environ Sci Technol. 2005; 39:1346–1353. [PubMed: 15787376]
28. Nutt MO, Heck KN, Alvarez P, Wong MS. Appl Catal, B. 2006; 69:115–125.
29. Wong MS, Alvarez P, Fang Y, Akcin N, Nutt MO, Heck KN. J Chem Technol Biotechnol.
30. Duff B. Langmuir. 1993; 9:2301–2309.
31. Jackson JB, Westcott SL, Hirsch LR, West JL, Halas NJ. Appl Phys Lett. 2003; 82:257–259.
32. Hu JW, Zhang Y, Li JF, Liu Z, Ren B, Sun SG, Tian ZQ, Lian T. Chem Phys Lett. 2005; 408:354–359.
33. Oldenburg SJ, Westcott SL, Averitt RD, Halas NJ. J Chem Phys. 1999; 111:4729–4735.
34. Sheppard N. Annu Rev Phys Chem. 1988; 39:589–644. [PubMed: 3075469]
35. Jugnet Y, Bertolini JC, Barbosa L, Sautet P. Surf Sci. 2002; 505:153–162.
36. Joyner P, Glockler G. J Chem Phys. 1952; 20:302–306.
37. Clotet A, Ricart JM, Pacchioni G. J Mol Struct (THEOCHEM). 1999; 458:123–129.
38. He ZH, Li Q, Leung KT. J Phys Chem B. 2005; 109:14908–14916. [PubMed: 16852888]
39. Wu ZL, Stair PC. J Catal. 2006; 237:220–229.
40. Baruya A, Gerrard DL, Maddams WF. Macromolecules. 1983; 16:578–580.
41. Lowry GV, Reinhard M. Environ Sci Technol. 2001; 35:696–702. [PubMed: 11349280]
42. Kopinke FD, Mackenzie K, Kohler R. Appl Catal, B. 2003; 44:15–24.
43. Baddeley CJ, Ormerod RM, Stephenson AW, Lambert RM. J Phys Chem. 1995; 99:5146–5151.
44. Azad S, Kaltchev M, Stacchiola D, Wu G, Tysoe WT. J Phys Chem B. 2000; 104:3107–3115.
45. Zaera F. Chem Rev. 1995; 95:2651–2693.
46. Wasylenko W, Frei H. J Phys Chem B. 2005; 109:16873–16878. [PubMed: 16853147]
47. Zaera F. Langmuir. 1996; 12:88–94.
48. Hansen EW, Neurock M. J Catal. 2000; 196:241–252.
49. Cremer PS, Somorjai GA. J Chem Soc, Faraday Trans. 1995; 91:3671–3677.

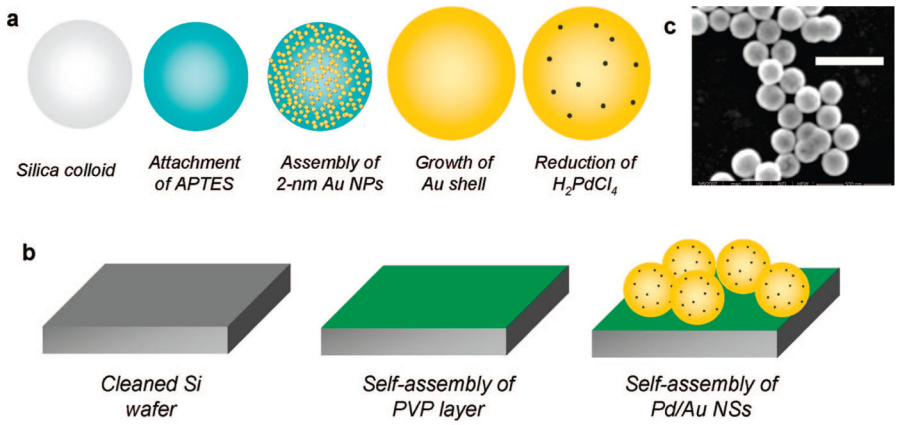

Figure 1.

(a) Synthesis schematic for catalytic Pd/Au NSs; (b) preparation schematic for NS SERS substrate; and (c) SEM of Pd/Au NSs (scale bar: 500 nm).

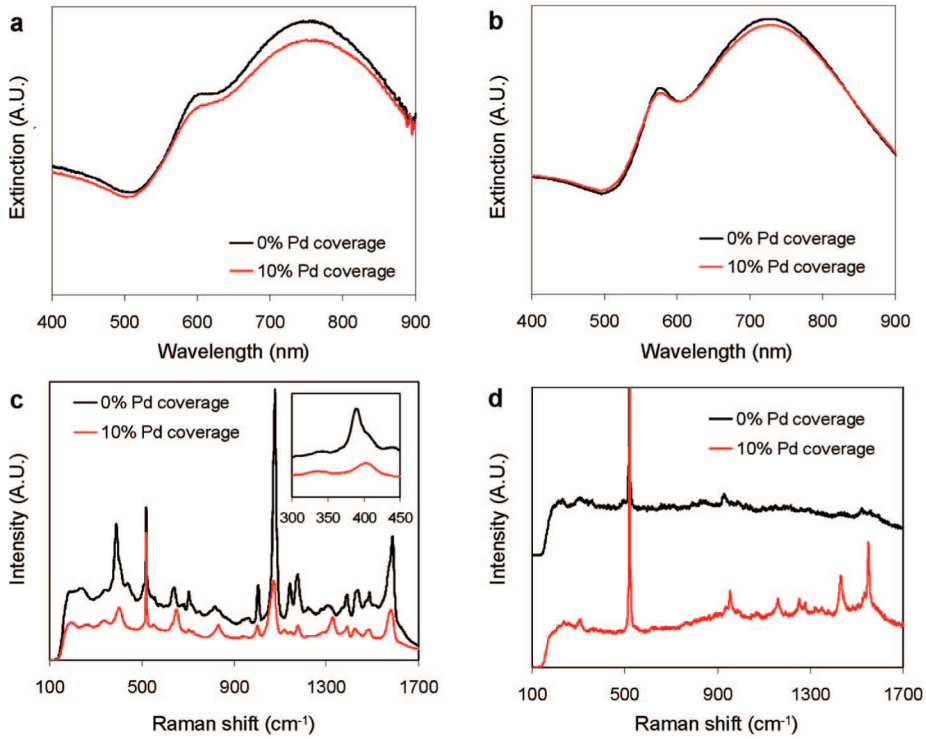

Figure 2.

(a) UV–vis spectra of Au NS and Pd/Au NS (10% Pd coverage); (b) calculated spectra of Au and Pd/Au NS; (c) spectra of pMA chemisorbed on Au NS and Pd/Au NS (10% Pd coverage) (inset: metal–S stretching region); (d) 1,1-DCE in H_2O (50.9 μM) on Au NS and Pd/Au NS (10% Pd coverage) (spectra offset for clarity). The Raman peak at ~500 cm^{-1} comes from the Si wafer, and small peaks in the 900–1000 and 1400–1600 cm^{-1} regions are from organic residuals prior to contact with 1,1-DCE.

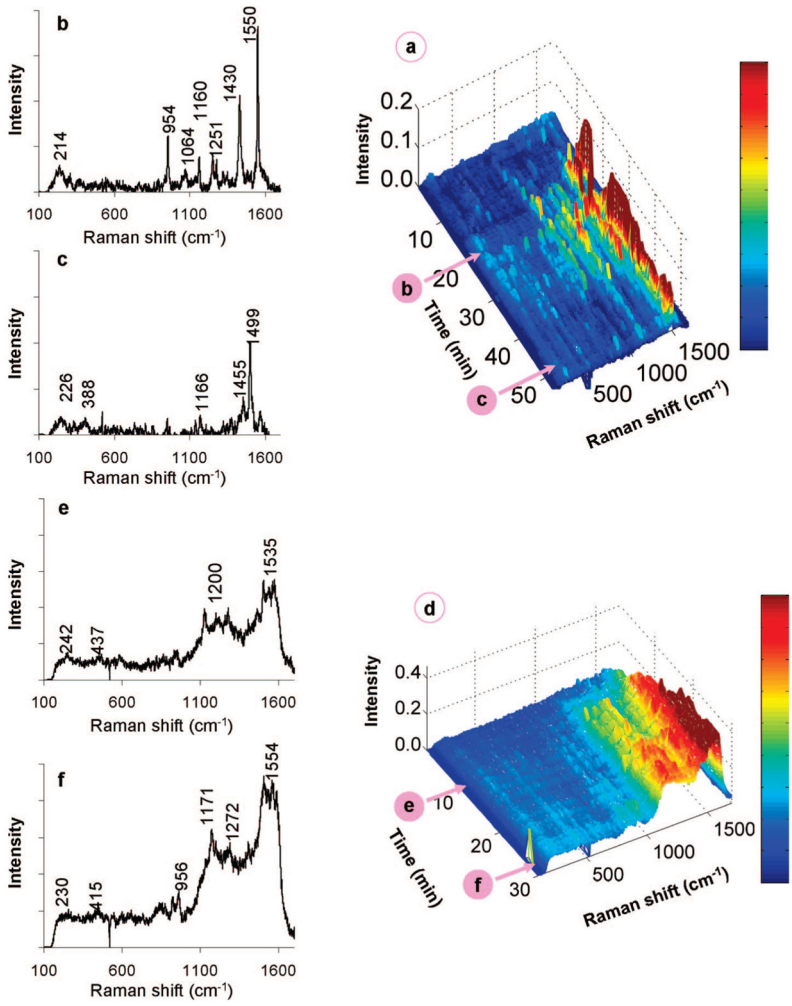

Figure 3.

(a) Waterfall plot of time-resolved spectra gathered from the chemisorption of 50.9 μM 1,1-DCE on Pd/Au NSs and (b,c) individual scans at 20 and 49 min after injection of 1,1-DCE solution. (d) Waterfall plot of time-resolved spectra gathered from the chemisorption of 254 μM 1,1-DCE and (e,f) individual scans at 10 and 28 min after injection of 1,1-DCE solution.

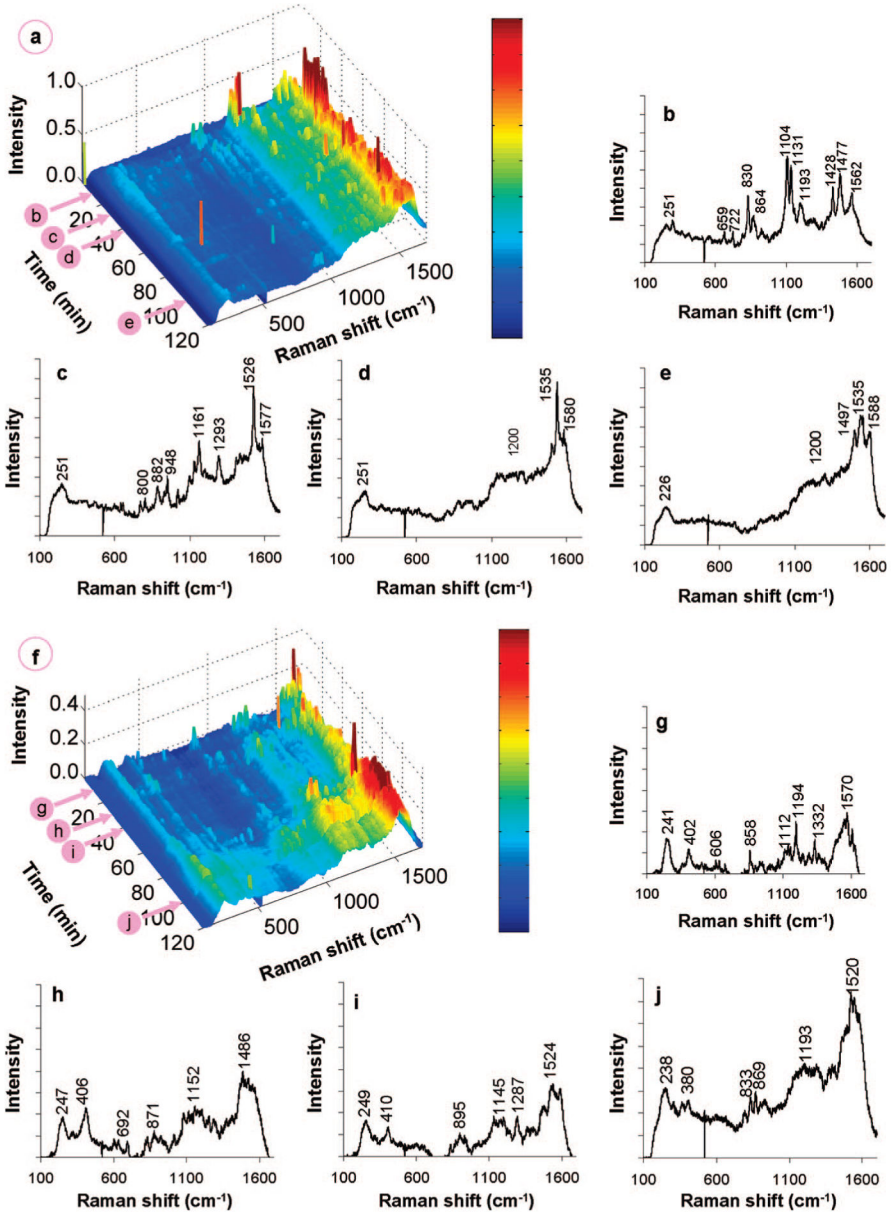

Figure 4.

(a) Waterfall plot of time-resolved spectra gathered from the reaction of 50.9 μM 1,1-DCE and 16.3 mM H_2 on Pd/Au NSs, and individual scans at 12, 30, 41, and 100 min (b, c, d, and e, respectively) after injection of 1,1-DCE/H_2 solution. (f) Waterfall plot of time-resolved spectra gathered from the reaction of 254 μM 1,1-DCE and 81.9 mM H_2 on Pd/Au NSs, and individual scans at 12, 30, 41, and 100 min (g, h, i, and j, respectively) after injection of 1,1-DCE/H_2 solution.

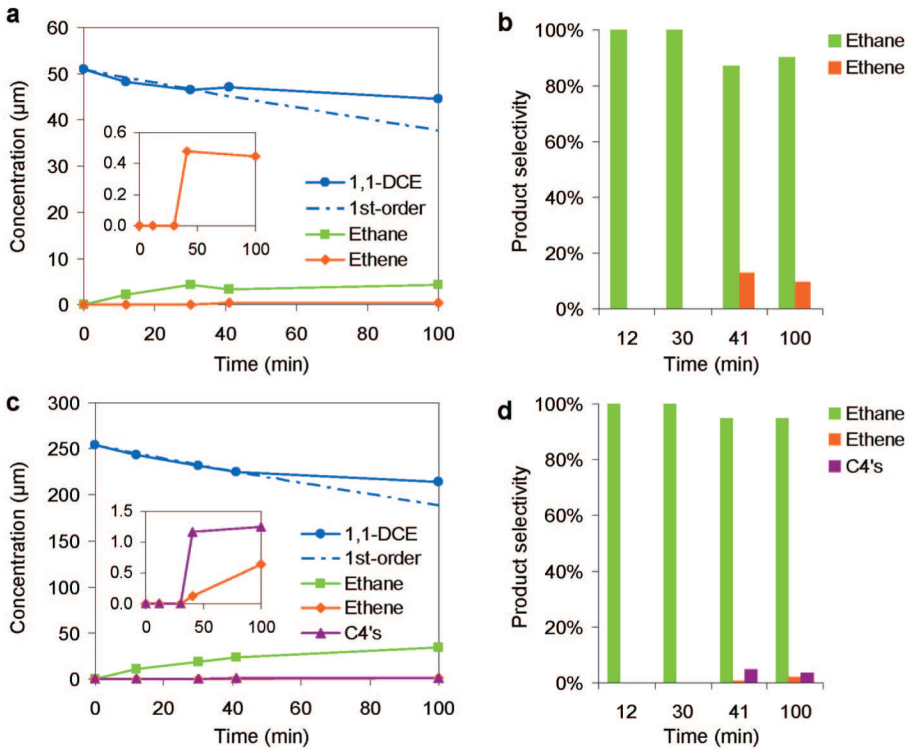

Figure 5.

(a) Concentration–time profiles and (b) product selectivities from the HDC reaction of 50.9 μM 1,1-DCE and 16.3 mM H_2, and (c) concentration–time profiles and (d) product selectivities from the HDC reaction of 254 μM 1,1-DCE and 81.9 mM H_2 using Pd/Au NS SERS substrate. The dashed traces show the expected 1,1-DCE concentrations using 0.003 min^{-1} as the first-order reaction rate constant.

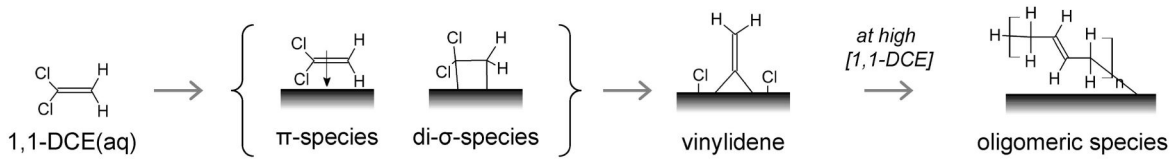

Scheme 1.

Proposed Surface Intermediates of 1,1-DCE after Adsorption on Pd/Au NS SERS Substrate Based on Spectroscopic Results[a]

[a] The arrows are drawn to indicate the probable sequence of identifiable species.

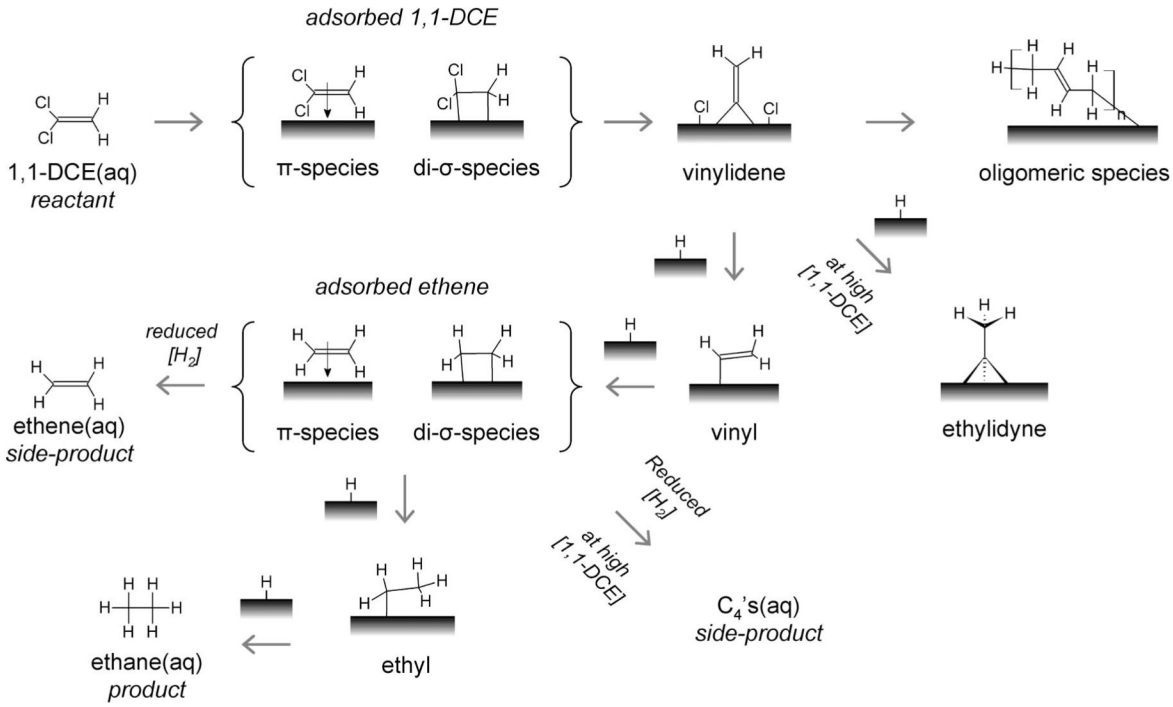

Scheme 2.

Proposed Surface Intermediates of 1,1-DCE and H_2 under Reactive Conditions on Pd/Au NS SERS Substrate Based on Spectroscopic Results[a]

[a] The aqueous-phase 1,1-DCE, ethane, C_4's, and ethane species were identified and quantified via gas chromatography. The arrows are drawn to indicate the probable sequence of identifiable species. The H surface atoms come from the dissociative adsorption of dissolved H_2.